Structure of Human Isovaleryl-CoA Dehydrogenase at 2.6 Å Resolution: Structural Basis for Substrate Specificity[†,||]

Karen A. Tiffany,[‡] David L. Roberts,[‡] Ming Wang,[‡] Rosemary Paschke,[‡] Al-Walid A. Mohsen,[§] Jerry Vockley,[§] and Jung-Ja P. Kim*[,‡]

Department of Biochemistry, Medical College of Wisconsin, Milwaukee, Wisconsin 53226, and Department of Medical Genetics, Mayo Clinic and Mayo Foundation, Rochester, Minnesota 55905

Received February 25, 1997; Revised Manuscript Received May 5, 1997[⊗]

ABSTRACT: Isovaleryl-CoA dehydrogenase (IVD) belongs to an important flavoprotein family of acyl-CoA dehydrogenases that catalyze the α,β-dehydrogenation of their various thioester substrates. Although enzymes from this family share similar sequences, catalytic mechanisms, and structural properties, the position of the catalytic base in the primary sequence is not conserved. E376 has been confirmed to be the catalytic base in medium-chain (MCAD) and short-chain acyl-CoA dehydrogenases and is conserved in all members of the acyl-CoA dehydrogenase family except for IVD and long-chain acyl-CoA dehydrogenase. To understand this dichotomy and to gain a better understanding of the factors important in determining substrate specificity in this enzyme family, the three-dimensional structure of human IVD has been determined. Human IVD expressed in *Escherichia coli* crystallizes in the orthorhombic space group $P2_12_12_1$ with unit cell parameters $a = 94.0$ Å, $b = 97.7$ Å, and $c = 181.7$ Å. The structure of IVD was solved at 2.6 Å resolution by the molecular replacement method and was refined to an *R*-factor of 20.7% with an R_{free} of 28.8%. The overall polypeptide fold of IVD is similar to that of other members of this family for which structural data are available. The tightly bound ligand found in the active site of the structure of IVD is consistent with that of CoA persulfide. The identity of the catalytic base was confirmed to be E254, in agreement with previous molecular modeling and mutagenesis studies. The location of the catalytic residue together with a glycine at position 374, which is a tyrosine in all other members of the acyl-CoA dehydrogenase family, is important for conferring branched-chain substrate specificity to IVD.

First hypothesized to exist in 1966 (Tanaka *et al.*, 1966), isovaleryl-CoA dehydrogenase (IVD) was purified from rat liver mitochondria in 1983 (Ikeda & Tanaka, 1983a). IVD is most reactive for a small, branched-chain substrate, catalyzing the conversion of isovaleryl-CoA (3-methylbutyryl-CoA) into 3-methylcrotonyl-CoA as the third step of leucine catabolism. This enzyme is a tetrameric flavoprotein which contains one molecule of flavin adenine dinucleotide (FAD) per monomer. Deficiency of IVD results in isovaleric acidemia (IVA), a life-threatening disorder in which leucine catabolism is blocked and organic acids accumulate in the body.

IVD is one of seven known mammalian acyl-CoA dehydrogenases, each with differing substrate specificities, that have been isolated from mitochondria. The four enzymes with straight-chain substrate specificities [short- (SCAD), medium- (MCAD), long- (LCAD), and very long- (VLCAD) chain acyl-CoA dehydrogenase] catalyze the first step of mitochondrial β-oxidation (Beinert, 1963; Aoyama *et al.*, 1994), while the other three enzymes [IVD, short/branched-chain acyl-CoA dehydrogenase (S/BCAD), and glutaryl-CoA dehydrogenase] are involved in amino acid catabolism (Ikeda & Tanaka, 1983b; Lenich & Goodman, 1986). cDNAs for all seven of these enzymes have been cloned and sequenced, and analysis of their DNA and predicted amino acid sequences suggests that they have evolved from a common ancestor, sharing 30−35% amino acid sequence identity (Tanaka *et al.*, 1987).

In addition to their sequence similarities, all acyl-CoA dehydrogenases exhibit similar biochemical properties and catalytic mechanisms. Except for the membrane-associated VLCAD, which is a homodimer, all acyl-CoA dehydrogenases are soluble homotetramers and contain one noncovalently bound flavin adenine dinucleotide (FAD) per monomer. Though all of these enzymes vary in their substrate specificities, they share an identical mechanism, catalyzing the α,β-dehydrogenation of their thioester substrates. The dehydrogenation reaction is initiated as a catalytic base from the enzyme abstracts the α-hydrogen of substrate in the form of a proton, with a concomitant transfer of the β-hydrogen from substrate as a hydride to the N(5) position of the isoalloxazine ring of the FAD, forming a *trans* double bond between the C_α and C_β of the fatty acyl-CoA substrate (Ghisla *et al.*, 1984). Ultimately, reducing equivalents are passed to the mitochondrial respiratory chain first via electron transfer flavoprotein (ETF) (Crane & Beinert, 1956), the physiological electron acceptor for all the acyl-CoA dehydrogenases, and second by ETF−ubiquinone oxidoreductase, a membrane-bound Fe-S flavoprotein (Ruzicka & Beinert, 1977).

Of all the members of the acyl-CoA dehydrogenase family, MCAD has been the most studied thus far, due mainly to its

[†] This work was supported by Grants GM29076 (J.-J.P.K.) and DK45482 (J.V.) from the U.S. Public Health Service.

[||] Atomic coordinates have been deposited in the Brookhaven Protein Data Bank, accession no. 1IVD.

* To whom correspondence should be addressed.

[‡] Medical College of Wisconsin.

[§] Mayo Clinic and Mayo Foundation.

[⊗] Abstract published in *Advance ACS Abstracts,* July 1, 1997.

S0006-2960(97)00422-4 CCC: $14.00

abundance in mitochondria and the high incidence of its deficiency manifesting as an inherited metabolic disease (Gregersen *et al.*, 1993). Powell and Thorpe (1988) identified E376 to be the active site base in MCAD by modification with a mechanism-based inhibitor 2-octynoyl-CoA, a finding subsequently substantiated by determination of the three-dimensional structures of MCAD and the MCAD−octanoyl-CoA complex (Kim & Wu, 1988; Kim *et al*., 1993). Of the 39 published amino acid sequences for enzymes belonging to this family, all but five have a glutamate at the position homologous to E376 of MCAD. Four of the five remaining enzymes contain a glycine residue at this position (rat IVD and human, rat, and mouse LCAD), while the fifth one contains an alanine residue (human IVD). In order to identify a possible alternative residue in the active site of LCAD which could function as the α-proton abstracting base in this enzyme, molecular modeling of human LCAD was performed using the pig MCAD coordinates as a template, since the two enzymes share 31% amino acid sequence similarity. From this modeling, it was proposed that E261 of human LCAD (corresponding to T255 in pig MCAD) could act as the catalytic base, and site-directed mutagenesis studies further supported this proposal (Djordjevic *et al.*, 1994). Since IVD also contains a glutamate residue at the position homologous to E261 of LCAD (E254 in IVD), while this position is a threonine, glycine, or alanine residue in all other family members, it was proposed that E254 is the catalytic base in IVD (Djordjevic *et al.*, 1994). Site-directed mutagenesis studies of this residue in human IVD (Mohsen & Vockley, 1995a) are consistent with this hypothesis.

With the recognition of life-threatening disorders such as IVA resulting from deficiencies of the various acyl-CoA dehydrogenases, there has been an increased interest in the structure and mechanism of these important flavoenzymes. Here we report the three-dimensional structure of human IVD complexed with CoA persulfide as determined by X-ray crystallography. Analysis of this structure has unequivocally identified E254 as the catalytic base and has enabled us to study the nature of the substrate specificity of this enzyme in detail.

MATERIALS AND METHODS

Crystallization. Human IVD was cloned, expressed, and purified as previously described (Mohsen & Vockley, 1995b). Briefly, the nucleotide sequence of the 5′ end of the human IVD cDNA was altered to accommodate *E. coli* codon usage in order to achieve a high level of expression. After expression, the cells were broken by sonication, and the enzyme was purified from the crude cell-free extract by a two-step procedure using DEAE-Sepharose followed by hydroxyapatite column chromatography. The purified IVD was dialyzed and concentrated against 50 mM potassium phosphate, pH 7.6. Initial crystallization was performed by vapor diffusion using the hanging drop method (McPherson, 1990) following the sparse matrix protocol (Carter & Carter, 1979). The initial screen yielded crystals in two conditions, and refinement of one condition resulted in single, diffraction-quality crystals of the purified protein. The final crystallization condition involved vapor diffusion using both hanging and sitting drop techniques by mixing equal volumes of the purified human IVD (16 mg/mL) with the precipitating solution [8% (w/v) poly(ethylene glycol) (PEG) 8000 and 100 mM Tris-HCl, pH 8.5] and equilibrating against the precipitating solution at 19 °C. Greenish yellow crystals were formed within 1 week and grew to the dimensions 0.5 × 0.3 × 0.3 mm within 1 month.

Table 1: Data Collection Statistics[a]

parameters	
resolution (Å)	2.6
total no. of reflections[b]	102598
unique reflections	43226
R_{sym} (%)[c]	8.02
completeness (%)	82.5
space group	$P2_12_12_1$
unit cell dimensions (Å)	
a	94.0
b	97.7
c	181.7
final *R*-factor (%)	20.7
R_{free} (%)	28.8
no. of water molecules	215
deviations in rms geometry	
bond length (Å)	0.009
bond angles (deg)	1.5

[a] The data set was collected using two crystals. [b] For all reflections with $I/\sigma > 0$. [c] $R_{sym} = \Sigma|I - \langle I\rangle|/\Sigma\langle I\rangle$ summed over all observations of all reflections.

Data Collection. The crystal was mounted in a glass capillary and diffraction data to 2.6 Å resolution were collected at 4 °C on an R-axis IIC image plate detector system with a Rigaku RU200 rotating anode generator. Still photographs indicated that the crystal belongs to the orthorhombic space group $P2_12_12_1$ with unit cell dimensions $a = 94.0$ Å, $b = 97.7$ Å, and $c = 181.7$ Å. On the basis of the assumption of one tetramer per asymmetric unit, the calculated V_m value is 2.4 Å^3/Da (Matthews, 1968). Diffraction data were collected using two different crystals to 2.6 Å resolution. The oscillation method was used for data collection, using 0.8° oscillation per frame at a crystal to detector distance of 200 mm, with $2\theta = 10°$. Data reduction and scaling were performed using the HKL package (Otwinowski & Minor, 1996), and data set statistics are given in Table 1.

Structure Determination. The structure of human IVD was solved by the molecular replacement method (Rossman & Blow, 1962) using the X-PLOR program package (Brünger, 1992). Human IVD shares 33.5% sequence identity with pig liver MCAD; therefore, the refined coordinates of native pig MCAD were used to construct the search model. Most of the MCAD residues were manually replaced with amino acids corresponding to that of IVD using TURBO-FRODO (Roussel & Cambillau, 1993) on a Silicon Graphics workstation. Residues were modeled as alanines in instances where the size of the MCAD side chains was smaller than the corresponding IVD sequence.

(1) Rotation Search. With an MCAD tetramer as the probe, a cross-rotation search was conducted using the Patterson search procedure as implemented in the X-PLOR package. Dimensions of the artificial cell which was searched were $a = b = c = 180$ Å, and the angular search interval was set to 1.5°. The 13 125 reflections whose intensities were greater than 5σ in the resolution range 15−4 Å were used.

(2) Translation Search. The translation search was carried out using the search molecule with Eulerian angles (6.70, 61.07, 243.54) that gave the highest peak in the rotation search and employed a standard linear correlation coefficient

Table 2: Molecular Replacement Solutions

Eulerian angles (deg)[a]			rotation function	Patterson correlation
θ_1	θ_2	θ_3		
Rotation Function				
6.70	61.07	243.54[b]	1.294	0.0715
61.37	56.25	305.90	1.297	0.0710
6.76	57.86	336.76	1.281	0.0687
64.56	53.04	32.16	1.276	0.0701
Translation Function				
vector (Å, along crystallographic axes *a*, *b*, and *c*)			peak height/σ	
30.29	40.17	44.42	20.6	

[a] The top four solutions are related by 222 symmetry consistent with the tetrameric molecule. [b] The search model with these Eulerian angles was chosen for the translation search.

Table 3: Refinement Progress

rounds of X-PLOR refinement	*R*-factor (%)	R_{free} (%)[a]	resolution (Å)	no. of reflections ($I/\sigma > 3.0$)	noncrystallographic symmetry weights (kcal mol^{-1} Å^{-2})
1−3	28.0	40.3	15−2.7	27761	NA
4−8	25.2	30.0	15−2.6	36353	300
9−10[b]	21.0	32.8	15−2.6	36353	150
11−13[c]	21.6	29.5	15−2.6	36353	5
14−15[d]	20.7	28.8	10−2.6	37968	5

[a] 2702 reflections, approximately 10% of the total, were used for calculating R_{free}. [b] Beginning with round 9, grouped *B*-factors were refined at the end of each cycle. Following the tenth cycle, the model contained the complete human IVD sequence. [c] Water molecules were added starting with cycle 11. [d] CoA persulfide was included in the final round of refinement. At this stage, 37 968 reflections between 10 and 2.6 Å resolution with $I/\sigma > 1.0$ were used.

between normalized, observed structure factors and normalized, calculated structure factors. Diffraction data with the resolution range between 15 and 4 Å were used. Searches were performed in the range *x*, *y*, and $z = 0-0.5$, with a sampling interval of 2 Å.

Structure Refinement. Refinement was carried out using iterative cycles of X-PLOR energy minimization followed by manual fitting and rebuilding on a Silicon Graphics workstation using TURBO-FRODO graphics software. In general, one round of X-PLOR refinement consisted of rigid body minimization, Powell positional refinement, a slow-cool simulated annealing beginning at 3000 K, and a second positional refinement. Later cycles also included refinement of the group and/or individual temperature factors. All four monomers in the asymmetric unit were refined using noncrystallographic symmetry (NCS) restraints until the *R*-factor was approximately 25%, at which point the NCS restraints were relaxed from a value of 300 to 150 kcal mol^{-1} Å^{-2}. When the *R*-factor reached 21%, the NCS restraints were further released to a value of 5 kcal mol^{-1} Å^{-2}, and all four monomers were modeled independently.

After each cycle of X-PLOR refinement, both $2|F_o| - |F_c|$ and $|F_o| - |F_c|$ difference Fourier maps were calculated. When needed to clarify problematic regions and to confirm the orientation of the catalytic base, simulated annealing difference Fourier omit maps were calculated starting at 1000 K. These maps were then used to carry out manual fitting and rebuilding of the model. At later stages of refinement, water molecules were assigned when densities greater than 3σ were observed in the $|F_o| - |F_c|$ electron density map which were within at least 3.3 Å of a potential hydrogen-bonding partner.

RESULTS

The Molecular Replacement Solution. The solutions for the molecular replacement searches are summarized in Table 2. Patterson correlation refinement of the 100 strongest peaks from the rotation search resulted in the emergence of four strong peaks which are related to one another by 222 symmetry corresponding to the tetrameric molecule. The search model with the Eulerian angles (θ_1, θ_2, θ_3) = (6.70, 61.07, 243.54) was chosen for the translation search. After the translation search, a single peak emerged with a peak height/σ of 20.6, yielding an initial *R*-factor of 52.9%.

Refinement of the Structure of IVD. The initial molecular replacement phases were improved, reducing the *R*-factor from 52.9% to 36.0% by employing one round of energy minimization consisting of rigid body, Powell positional, and simulated annealing refinement. At this stage, manual rebuilding of the model was performed. In the regions where alanines were initially modeled due to incongruous residues between the MCAD model and IVD, the correct IVD residues were inserted when electron density was observed in the difference Fourier maps. After ten iterative cycles of energy minimization refinement followed by manual model rebuilding, the entire human IVD sequence was correctly incorporated into the model. The *R*-factor at this point was 21.0%, with a free R-factor of 32.8%, for the 36 353 reflections between 15 and 2.6 Å resolution with $I/\sigma > 3.0$. Table 3 indicates the refinement progress with the structure of human IVD. After a total of 16 repetitive cycles of energy minimization refinement followed by manual adjustment of the model, the final *R*-factor without water molecules is 22.2%, with a free *R*-factor of 29.2% for the 37 968 reflections between 10 and 2.6 Å resolution with I/σ greater than 1.0. After the addition of 215 water molecules, the *R*-factor dropped to 20.7%, with a free *R*-factor of 28.8%. The final model of the human IVD tetramer, complete with four FAD molecules, contains 12 109 non-hydrogen atoms, not including the 215 water molecules. Of the 394 amino acid residues in a monomer of mature human IVD, all but five (the first four N-terminal residues and the final C-terminal residue) have well-defined densities which allow for the proper assignment of their positions.

The statistics for the IVD model are reported in Table 1. The average *B*-factor value for the main-chain polypeptide backbone is 12 Å^2, and the average side-chain *B*-factor is 16 Å^2. Ramachandran plot analysis indicates that, for main-chain dihedral angles, 90% of the residues reside in the most favored regions and none are observed in disallowed regions. The root mean square (rms) deviations of the bond lengths and bond angles of the IVD model are 0.009 Å and 1.5°, respectively, and the rms deviation between main-chain atoms of IVD monomers of the tetramer within the asymmetric unit is 0.10 Å.

Description of the Structure of IVD. The overall structure of IVD is similar to that of MCAD and other acyl-CoA dehydrogenases whose three-dimensional structures have been determined previously (Kim & Wu, 1988, 1993; Djordjevic *et al.*, 1995, Kim, unpublished results). The rms deviation between the main-chain atoms of human IVD and pig MCAD is 1.21 Å and between human IVD and butyryl-CoA dehydrogenase (BDH, a bacterial homolog of SCAD; Djordjevic *et al.*, 1995) is 1.01 Å. As with the other known

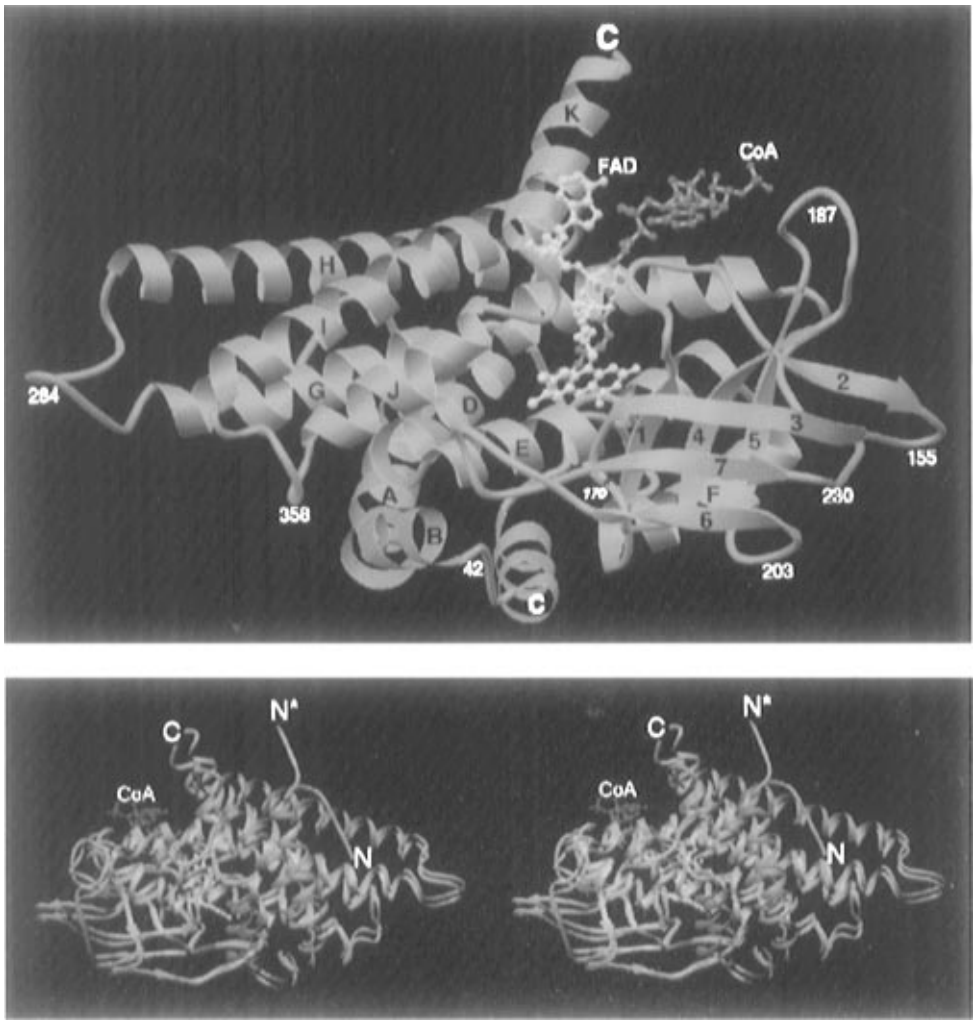

FIGURE 1: (A, top) Ribbon diagram of a monomer of IVD with bound CoA persulfide. Using the nomenclature derived for MCAD, the α-helices are labeled in alphabetical order and the β-strands are labeled in numerical order from the N- to the C-terminal ends. The FAD (yellow) and CoA persulfide (red) are represented by balls and sticks. The smaller numbers are used to help follow the polypeptide tracing. G170, which represents a mutation site in IVD, is also indicated (∗). All figures were made with the program RIBBONS (Carson, 1996). (B, bottom) Stereo diagram of a superposition of monomers from IVD and MCAD. IVD (cyan ribbon) and MCAD (lavender ribbon) were overlapped using the RIGID feature of the TURBO-FRODO program (Roussel & Cambillau, 1993). The N-termini of IVD and MCAD are labeled as N and N*, respectively. The CoA persulfide (red) and FAD (yellow) of IVD are represented by balls and sticks. The orientation is looking at the "back side" of IVD and MCAD, with the molecules rotated 180° compared to the orientation shown in panel A.

structures of acyl-CoA dehydrogenases, each monomer of IVD consists of three domains: an α-helical N-terminal domain, a β-sheet domain in the middle, and a second α-helical domain at the C-terminus. The FAD has an extended conformation and is located between the middle and C-terminal domains of one monomer and the C-terminal domain of a neighboring monomer. A ribbon diagram of a monomer of IVD, with helix and strand names labeled according to the nomenclature devised for MCAD (Kim *et al.*, 1993), is shown in Figure 1A.

While the overall fold and topology of IVD are similar to the other known structures of acyl-CoA dehydrogenases, there are some key structural differences which are likely to be significant. These differences occur primarily in the N-terminal segment and loop regions (Figure 1B). A marked difference exists between the structures of the mature human IVD and the mature pig MCAD in the first 15 N-terminal residues. The amino acid residues which precede G12 in human IVD (corresponding to E15 in pig MCAD) are oriented in a direction almost 180° away from that of the corresponding N-terminal residues of pig MCAD. Moving past the N-terminus, there is a shift between the α-carbon atoms of loop BC (see Figure 1A for nomenclature) in IVD and those of MCAD, which is as large as 5.4 Å in some places. This shift between the corresponding α-carbon atoms of IVD and MCAD is further propagated through helix C (an rms deviation of approximately 2 Å) and the connecting loop between helices C and D, yielding differences between IVD and MCAD ranging from 2.8 to 3.5 Å in the positions of the α-carbon atoms of this loop. There is also a bulge in helix E of human IVD that is not present in the structure of pig MCAD. This bulge results in a decrease in the width of the substrate binding pocket of approximately 1.5 Å in IVD compared to that of MCAD, which is similar to what is seen in BDH. The loop connecting β-strands 4 and 5 extends farther into the MCAD structure compared to IVD. Finally, differences exist in the loops between helices H and I of MCAD and IVD. As in the case of the loop between β-strands 4 and 5, the loop connecting helices H and I is longer in MCAD than in IVD. Two cysteine residues in IVD (C318 and C323) are located close to one another in this loop and appear to form a disulfide bond in the crystal structure. In order to confirm this observation, a difference Fourier omit map around these two cysteine residues was

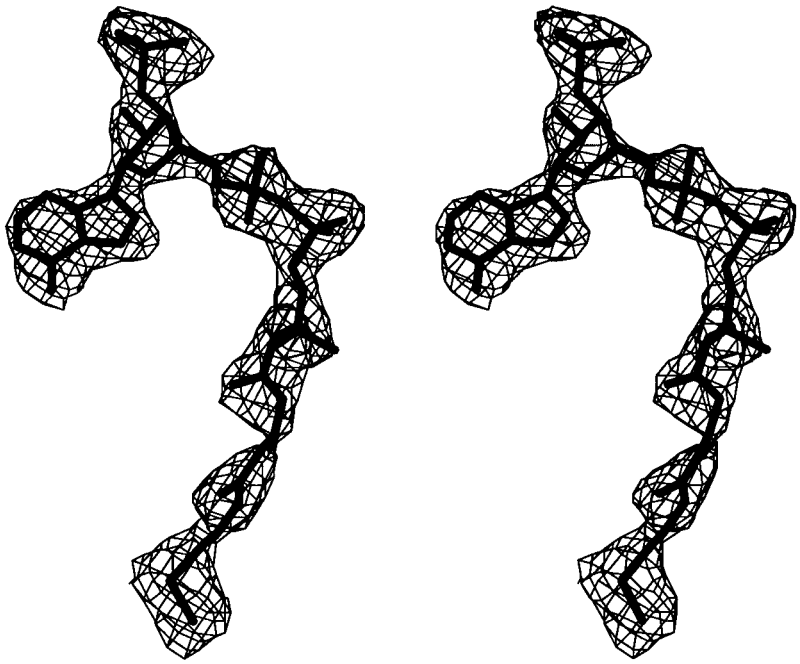

FIGURE 2: Stereo diagram of a model of CoA persulfide fitted into the final electron density map. A $2|F_o| - |F_c|$ difference Fourier map was calculated using the X-PLOR program and displayed using TURBO-FRODO. The map is contoured at 1.2σ.

calculated, and the results confirm that electron density bridges the two γ-sulfurs of these cysteines (3σ) that are separated by a distance of approximately 2.1 Å. Once this observation was made, these two sulfhydryls were refined as a disulfide linkage.

The Active Site. Both $2|F_o| - |F_c|$ and $|F_o| - |F_c|$ difference Fourier maps yielded well-defined tubular density in the active site near the FAD ring in the IVD monomers. The shape of this density and the greenish color of the IVD crystals suggest that this density represents a molecule of CoA persulfide ($CoASS^-$). Similar to the density observed in the cases of octanoyl-CoA bound to MCAD (Kim *et al.*, 1993) and acetoacetyl-CoA bound to BDH (Djordjevic *et al.*, 1995), the pantetheine moiety of this density runs parallel to the ribityl portion of the FAD. A molecule of CoA persulfide was therefore modeled in the monomers of IVD where this density was observed (Figure 2).

The substrate binding pocket of IVD is similar to those observed in the structures of MCAD and BDH. The opening to the CoA binding pocket, where the adenosine diphosphate portion of the CoA moiety lies, is exposed to the solvent, while the bottom of this pocket, which surrounds the fatty acyl segment of the CoA thioester substrate, is comprised of mainly hydrophobic amino acid residues of the polypeptide along with the isoalloxazine ring of FAD. The residues that line the active site cavity and substrate binding pocket are located on the loops connecting β-strands 1 and 2 and β-strands 4 and 5, the loops between helices J and K and between helices H and I, and parts of helices E and G (Figure 1A).

There are several key residues involved in binding to the adenosine portion of the fatty acyl-CoA moiety (Figure 3A). As in the other structures of acyl-CoA dehydrogenases, the amino acid residues D252 and S190 make hydrogen bond interactions with the N_6 and with the 3′-phosphate of the adenosine, respectively (BDH has an asparagine residue in the position homologous to S190). However, unlike MCAD, which has an arginine residue that is also involved in forming a hydrogen bond with the N_6 of the adenine, the corresponding residue in IVD at position 323 is a cysteine. In addition to S190 forming a hydrogen bond with the 3′-phosphate of the adenosine, IVD contains two additional residues, R191 and Y245, which are also involved in hydrogen bonding with this 3′-phosphate (Figure 3A). The corresponding residues in MCAD (Kim *et al.*, 1993), BDH (Djordjevic *et al.*, 1995), and SCAD (Kim, unpublished results) are all lysines (except BDH, which has a histidine residue corresponding to R191 of IVD) which are oriented away from, and do not appear to interact with, the 3′-phosphate moiety.

As depicted in Figure 3B, the amino acid residues that line the fatty acyl binding pocket of human IVD are mostly hydrophobic, including residues L95, A99, L103, T168, L258, L370, Y371, G374, and A375. The depth of the binding cavity is shallower in IVD compared to that of MCAD but comparable to that of BDH and SCAD. This observation is consistent with experimental kinetic data that show minimal activity for substrates longer than six carbons in IVD, BDH, and SCAD. While the depth of the binding pocket is shallower than that of MCAD, the binding pocket is wider in IVD than in MCAD; this allows for the accommodation of a branched-chain substrate in IVD. This change in the width is due to the presence of a glycine residue at position 374, the corresponding position to which is a tyrosine residue in all other acyl-CoA dehydrogenases (Figures 3B and 4; see Discussion).

Finally, this structure of human IVD has conclusively identified the catalytic base. By modeling isovaleryl-CoA into the density for the CoA persulfide, it is observed that E254 is located in the active site near the location of the $C_\alpha - C_\beta$ bond of the substrate (Figure 5). The distance between the carboxylate of E254 and C_α of the CoA is 3.3 Å, and the distance between the N_5 of the FAD and C_β of the CoA is 3.5 Å. Taken together with prior mutagenesis studies (Mohsen & Vockley, 1995a), this confirms that E254 of IVD is indeed the catalytic base responsible for substrate α-proton abstraction and is the homolog of E376 of MCAD.

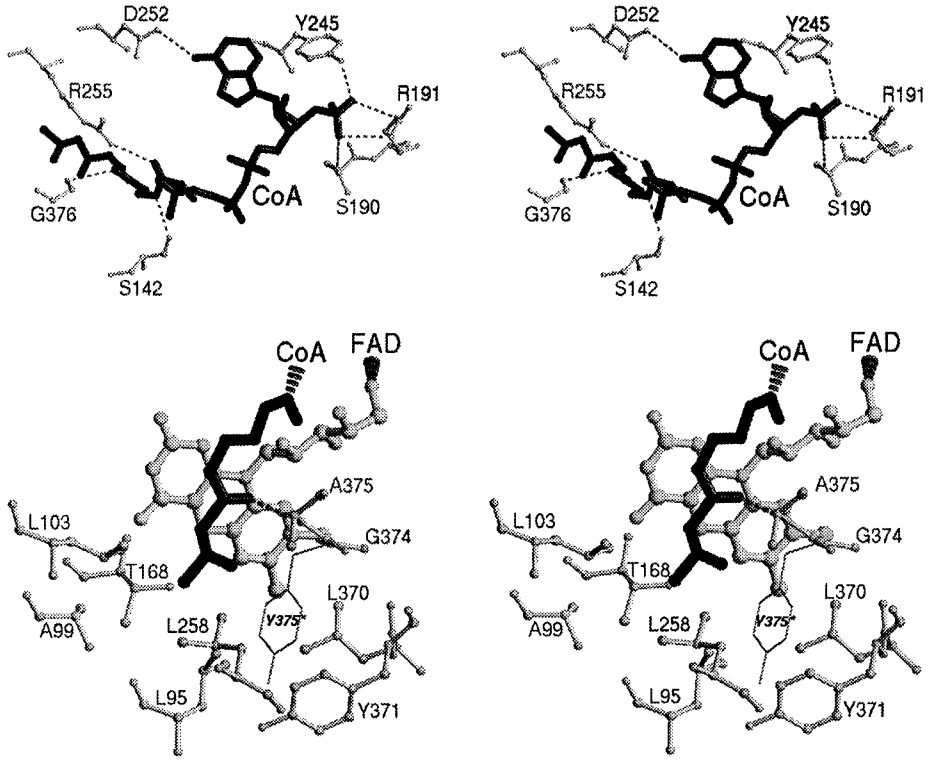

FIGURE 3: Stereo diagram of residues involved in substrate binding in IVD. Isovaleryl CoA (dark sticks) was modeled into the active site of IVD using the density observed for CoA persulfide. The branched substrate was modeled by minimizing steric hindrance. (A, top) Residues involved in binding to the adenosine and pantetheine moiety of the CoA are shown (light ball and sticks). Dotted lines represent potential hydrogen bonds. (B, bottom) Residues located in the vicinity of the fatty acyl portion of the CoA moiety are shown (smaller ball and sticks). The isoalloxaxine ring and ribityl portions of the FAD cofactor are shown (larger ball and sticks), along with the fatty acyl portion of the CoA moiety (dark sticks). Residues involved in conferring substrate specificity are indicated. Y375*, which is the invariant tyrosine residue found in all ACDs except for IVD, was modeled into the structure by overlaying pig MCAD and IVD (thin lines). The hydrogen bond between the amide nitrogen of A375 and the substrate is indicated by dotted lines.

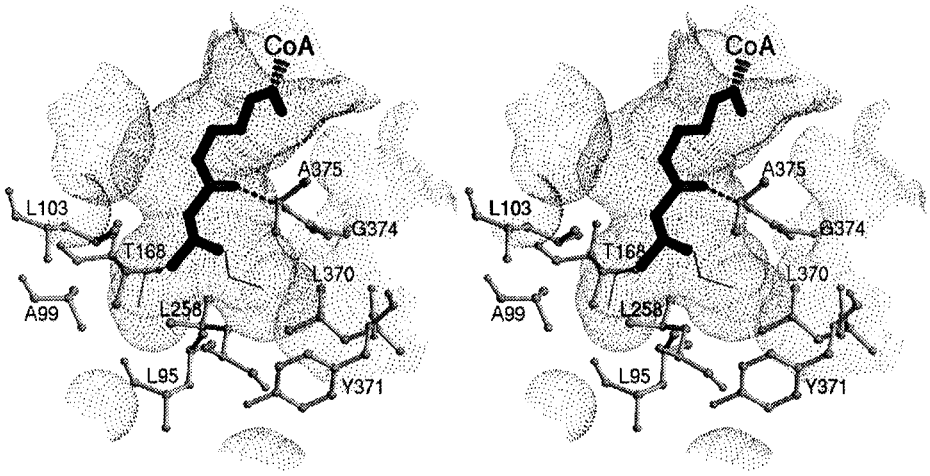

FIGURE 4: Solvent-accessible surface area at the "base" of the active site cavity of IVD. Isovaleryl-CoA was modeled into the structure of IVD into the density that was observed for CoA persulfide. The solvent-accessible surface area was calculated in the absence of bound CoA ligand. The radius of the probe used to generate the solvent-accessible area was 1.4 Å. The fatty acyl portion of the isovaleryl-COA is shown (dark sticks), as well as two possible conformations for the fatty acyl portion of hexanoyl-CoA (light lines). Residues that line the cavity and confer substrate specificity are also shown (light ball and sticks). The view is identical to that shown in Figure 3B. From this figure, it is clear that the fatty acyl portion of hexanoyl-CoA can adopt two conformations, due to the lack of a tyrosine residue at position 374 in IVD (Figure 3B).

DISCUSSION

Structural studies on related enzymes of the acyl-CoA dehydrogenase family have revealed the structural basis for their mechanism of enzyme action and provide insight as to how these enzymes have evolved to accommodate their specific substrates. In comparing the structures of these homologous enzymes, it is crucial to analyze not only their similarities but also their differences. Conserved amino acid residues may indicate factors that are important for common properties shared by members of the family, such as catalytic function and overall structure. On the other hand, divergent residues may, at least in part, be responsible for the enzymatic characteristics which differentiate these enzymes. While the three-dimensional structure of human IVD is very similar

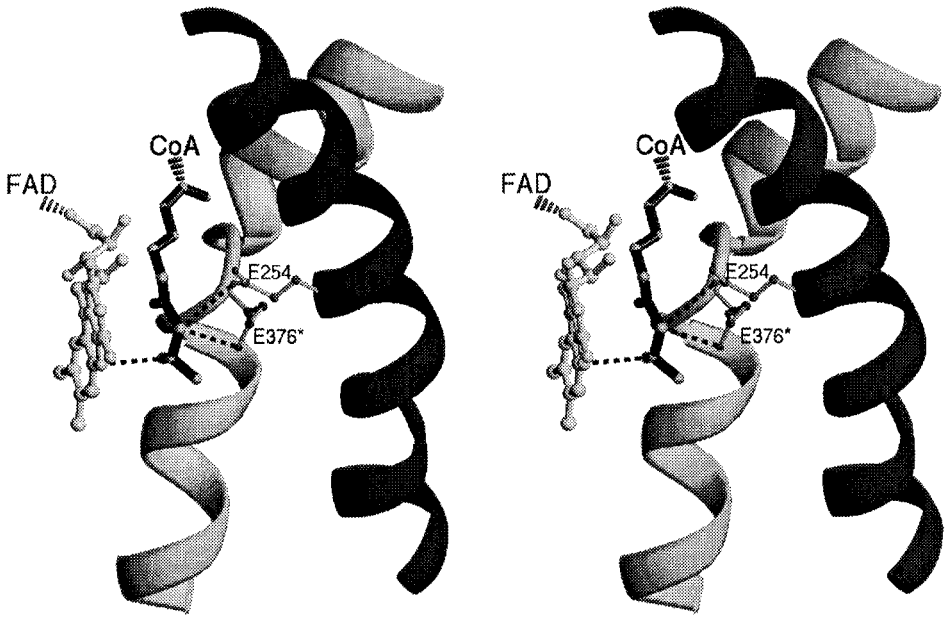

FIGURE 5: Comparison of the location of the active site base in IVD and MCAD. The isoalloxaxine and ribityl portion of the FAD cofactor (larger ball and sticks), along with the fatty acyl portion of the isovaleryl CoA substrate (dark sticks), is shown. Helix G of IVD, which contains the catalytic base E254, is represented by the dark ribbon, while helices J and K of MCAD, including the loop between them which contains the catalytic base E376*, are represented by the lighter ribbon. The smaller ball and sticks represent E254 of IVD, as well as the active form of E376 of MCAD (denoted by E376*). Dotted lines indicate the points of proton abstraction, from C2 of the substrate to the catalytic base (either E254 or E376*), and the hydride transfer from C3 of thesubstrate to the N5 of the isoalloxazine ring of FAD.

to that of the known structures of other acyl-CoA dehydrogenases, subtle but significant differences provide the first insight into the nature of branched-chain substrate specificity in this family of enzymes.

Structural Differences between IVD and MCAD. In MCAD and BDH, both the N- and C-terminal ends of one dimer extend into the neighboring dimer and are involved in dimer−dimer interactions, stabilizing the active tetramer. Similarly, the C-termini of an IVD dimer extend into the other IVD dimer. However, unlike MCAD and BDH, the N-terminus of IVD is oriented away from the dimer−dimer interface and therefore does not interact with the neighboring dimer. Several possibilities could account for the differing orientation of the N-terminus of IVD as compared to MCAD. Upon examination of the molecular packing, it is apparent that crystal packing forces do not influence the orientation of the N-terminus of IVD. Rather, it appears that the primary sequence of IVD plays a key role in determination of the N-terminal folding. Comparison of the residues of IVD and MCAD in this region reveals poor sequence homology between all members of the acyl-CoA dehydrogenase family. Structurally, the N-terminus of IVD folds back within the same monomer, forming several hydrogen bonds and salt bridges within the N-terminus and neighboring residues (Figure 1B). In contrast, MCAD lacks many of these analogous residues and, therefore, extends deep into the neighboring subunit. The N-termini of adjacent dimers interact through a hydrophobic portion of the N-terminal region which includes the sequence S11, G12, F13 (MCAD numbering). This region in IVD is more acidic, consisting of two consecutive aspartic acid residues (D7 and D8, IVD numbering). In addition, D7 forms a salt bridge with an arginine residue (R308) within the same monomer. Thus, it appears that the primary sequence of IVD plays a key role in dictating the orientation of the N-terminus, leading to a position that balances its negative charges. Another significant structural difference between IVD and MCAD is that, as in the case of BDH and rat SCAD (Djordjevic *et al.*, 1995; Kim, unpublished results), there is a single residue insertion (N102) in the sequence of IVD in helix E compared to that of MCAD. This results in a bulge in helix E of IVD, which causes helices E and G to be closer to one another in IVD than in MCAD. Since the acyl-CoA substrate binds between helices E and G, the binding cavity of the fatty acyl moiety in IVD is shallower than that of MCAD. It is, in part, the residues located on these two helices which are responsible for substrate specificity.

The loop region between helices H and I is approximately 15 Å away from the catalytic site; however, it is close to the binding site of the adenine moiety of the substrate. The structure of IVD reveals a disulfide bond between residues C318 and C323 in this loop. The presence of cysteines in this region is unique to IVD among the members of the acyl-CoA dehydrogenase (ACD) gene family; however, the physiological relevance of this disulfide bond is unclear. The high cellular concentration of glutathione (Ziegler, 1985) suggests that these two cysteine residues would most likely exist in their reduced form *in vivo*. Furthermore, incubation of IVD with 5 mM glutathione for 24 h does not alter its measured enzyme activity (data not shown). Finally, DNA sequencing data show that C323 in rat and mouse IVD is an isoleucine (Matsubara *et al.*, 1989; Vockley, unpublished data). Thus, it seems unlikely that the disulfide bond in human IVD plays an important role in modulating enzymatic activity *in vivo* in the context of the normal cellular milieu.

The Bound Ligand Is Consistent with That of CoA Persulfide. As refinement of the human IVD structure progressed, difference Fourier maps revealed an elongated, tubular density in the substrate binding pocket, although no substrate or substrate analog was added at any time during purification or crystallization of this enzyme. The observed density extends from the opening of the CoA binding pocket

through the region in which the pantetheine moiety lies but is truncated abruptly upon entering the fatty acyl binding pocket. The density is sufficient to accommodate CoA persulfide, which is known to bind tightly to acyl-CoA dehydrogenases (Williamson *et al.*, 1982). When isolated from *Megasphaera elsdenii*, BDH exhibits a bright green color instead of the characteristic yellow color of flavoproteins (Williamson & Engel, 1984). This green color, also observed in mammalian SCAD (Mahler, 1954; Steyne-Parve & Beinert, 1958; Hoskins, 1966; Battaile *et al*., 1996) and in an active site mutant (E376Q) of human MCAD (Bross, *et al.*, 1990), is due to a charge-transfer complex species with a tightly bound CoA persulfide (Williamson *et al.*, 1982). Purified IVD and its crystals also have a green color and exhibit a broad absorbance band from approximately 650 to 700 nm (spectrum not shown), although the magnitude of this band is less than seen with SCAD. This is consistent with the supposition that a charge transfer complex is formed with a tightly bound CoA persulfide ($CoASS^-$; Williamson *et al.*, 1982). Close inspection of the "green" enzymes reveals that they all lack a negative charge in the substrate binding pocket that may contribute to a tighter binding of the negatively charged $CoASS^-$ molecule. MCAD contains two glutamate residues in the active site pocket, E376 and E99, while IVD, BDH, SCAD, and the mutant MCAD (E376Q) all contain only one acidic residue (E254, E367, E374, and E99, respectively). In IVD, BDH, and SCAD, the residues corresponding to E99 of MCAD are G98, S91, and S99, respectively. This observation is consistent with the idea that the negative charge of the CoA persulfide may preclude it from tightly binding to MCAD due to the two acidic residues, E376 and E99 but that it can bind quite tightly to IVD, BDH, and SCAD, all of which have only one glutamate within the binding pocket. In the case of the E376Q mutant of MCAD, the acidic E99 still exists but the other negatively charged residue, E376, is mutated to the neutral residue glutamine.

The Structural Basis for Short, Branched-Chain Substrate Specificity Is Revealed. The substrate specificity of IVD differs from the other ACDs in two important characteristics: the chain length of the substrate and the branch point of the substrate. Although IVD and SCAD (BDH) can both utilize valeryl-CoA as substrate, IVD shows maximal activity with the branched-chain substrate isovaleryl CoA, which contains a methyl group at the C_β position. For straight-chain substrates, MCAD has broad specificity, ranging from C_4 to C_{12} CoA (Nandy et al., 1996). In contrast, the specific activity of IVD for C_8-CoA is only 1% and for C_4-CoA is 20% of the activity for its optimum substrate, isovaleryl CoA (Mohsen & Vockley, 1995a). The structure of human IVD reveals several characteristics that play an important role in determining these differences in substrate specificity.

Many of the residues lining the fatty acyl binding site (including A99, L103, T168, and Y371, also shown in Figure 3B) are identical in human IVD and pig MCAD. However, due to differences in the conformations of helices E and G, the fatty acyl binding pockets are shallower in IVD and BDH compared to that of MCAD. So, even though residues 99 and 103 in helix E are conserved between IVD and MCAD, the position of the α-carbons of these residues is closer to the substrate in IVD than in MCAD. L95, located in helix E, also contributes to making the substrate binding pocket shallower. Not only is the α-carbon of L95 (located within the bulge in helix E of IVD) closer to the substrate but the side chain of leucine is bulkier than the side chain of the homologous T96 in pig MCAD. BDH, another enzyme whose optimum substrate is shorter than that of MCAD, also has this insertion in helix E, resulting in a similar bulge. Furthermore, the residue corresponding to L95 of IVD is an isoleucine in BDH, which is also bulkier than the T96 of MCAD. Another residue that is important in conferring short-chain specificity in IVD is L258, which is located in helix G. As in BDH (Djordjevic *et al.*, 1995), helix G in IVD is straighter and closer to the substrate than the corresponding helix in MCAD. From modeling studies in which a molecule of octanoyl-CoA is overlaid onto the IVD structure (data not shown), it is apparent that the side chain of L258 would lie too close to the C7 and C8 atoms (1.6 and 1.8 Å, respectively) of the CoA substrate to accommodate this substrate in the active site cavity, and so the longest substrate that could be accommodated by IVD is hexanoyl-CoA (Figure 4). In contrast, the homologous residue in MCAD is the less bulky V259. Taken together, the structural differences that exist in these regions between IVD and MCAD, along with the nature of the residues that line the active site pocket, confer a shorter chain substrate specificity in IVD as compared to MCAD.

Two differences in side chains between human IVD and pig MCAD are noted to be important in conferring branched-chain specificity in IVD. G374 and A375 line the substrate binding pocket in IVD, whereas the corresponding residues in pig MCAD are Y375 and E376, respectively. The position corresponding to Y375 is conserved in all known acyl-CoA dehydrogenases (including LCAD and S/BCAD) with the exception of IVDs from various species. A glycine residue at this position in IVD eliminates steric repulsion with the 3-methyl group of isovaleryl-CoA, supporting the proposal that the tyrosine is important in conferring straight-chain specificity (Nishina *et al.*, 1995). The distance from the α-carbon of G374 to the 3-methyl group of the substrate is 5.5 Å. If the substitution G374Y is made, keeping the same orientation as that of Y375 of MCAD, the distance between the C_γ of this residue and the 3-methyl group of isovaleryl-CoA would be only 1.8 Å (Figure 4). Analysis of the solvent-accessible surface area of IVD in the absence of bound CoA analogs shows that the lack of a tyrosine residue at position 374 leads to a branched configuration of the IVD active site pocket, which can therefore accommodate branched-chain substrates (Figure 4). A similar analysis for MCAD shows that MCAD cannot accommodate branched chains at the position C_3, due to van der Waals interactions between the branched chain and Y375 (see Figure 3B for the position of Y375; Lee *et al.*, 1996). The catalytic rate of MCAD toward isovaleryl-CoA is 0.25% that of the activity for its optimal substrate, octanoyl-CoA (data not shown). While the solvent-accessible surface of IVD shows that the active site is shallower than that of MCAD, the width is such that the straight-chain C_6-CoA substrate could lie in two conformations: one that is similar to the conformation observed in MCAD or one in which the C_6 substrate binds in the space normally occupied by Y375 of MCAD, in a way that is quite different than in MCAD (Figure 4). The binding pocket in IVD cannot readily accommodate anything longer than C_6-CoA, thus explaining the low catalytic rate which IVD displays with these substrates.

Although the Catalytic Mechanisms Are Similar, the Topographical Location of the Catalytic Base in IVD Is Different from Other Acyl-CoA Dehydrogenases. In the other acyl-CoA dehydrogenases whose structures are known, the catalytic base is a glutamic acid residue located on the loop connecting helices J and K at the position corresponding to 375 in the IVD primary sequence. Sequence comparisons among all the members of the acyl-CoA dehydrogenase family show that the location of this catalytic base is conserved in all but two of the acyl-CoA dehydrogenases, LCAD and IVD. In these later cases, molecular modeling studies together with site-directed mutagenesis have suggested that the catalytic glutamate in LCAD (E261) and the corresponding glutamate in IVD (E254) are located approximately 115 residues away in the primary sequence in helix G. This glutamic acid residue, unique in LCAD and IVD, is either a threonine, glycine, or alanine in other members of the family. Figure 5 illustrates the positions of E254 of IVD and E376 of MCAD with respect to substrate.

To assess the ability of a catalytic base to abstract a proton, two elements are considered: the distance of the base from the substrate (*i.e.*, the proton to be extracted) and the orientation of this base with respect to the C−H bond to be cleaved (Gandour, 1981). Mutagenesis studies on MCAD using the double mutant E376G/T255E, which mimics the active site base position of IVD and LCAD, shifted the substrate specificity of MCAD for longer straight-chain substrates, analogous to activity observed for LCAD (Nandy *et al.*, 1996). Crystallographic studies on this enzyme showed that the catalytic base, now E255, was approximately 4.0 Å away from the proton to be abstracted, which is longer than the 2.7 Å distance found in the wild-type enzyme (Lee *et al.*, 1996). This observation is consistent with enzymatic studies that determined the double mutant to be less efficient at catalysis than the wild-type enzyme, in part because of the distance from E255 to the substrate. By modeling isovaleryl-CoA into the density observed for CoASS$^-$ in the IVD structure, the distance between the carboxylate oxygen of E254 and the C_α of the substrate is about 3.0 Å in IVD, which is comparable to the distance observed in the MCAD and BDH structures. Therefore, unlike the double mutant form of MCAD, the distance from the catalytic base to the substrate in IVD does not appear to affect the catalytic efficiency in IVD.

The second factor influencing catalytic efficiency is the angle at which the catalytic base approaches the substrate. From the crystal structure of MCAD in the presence of C_8-CoA, the carbonyl oxygen of the CoA substrate forms hydrogen bonds with the 2′-hydroxyl of the FAD ribityl chain and the main-chain amide nitrogen of E376, thus "orienting" the protons to be abstracted with respect to the catalytic base and FAD. Crystallographic studies on the E376G/T255E double mutant of MCAD showed that, in the mutant enzyme, the catalytic base E255 approaches the substrate at an angle approximately 40° different from in the wild-type enzyme (Lee *et al.*, 1996). Modeling of isovaleryl-CoA into the active site of IVD shows that, due to the presence of a branched methyl group on the β-carbon of the substrate, the positioning of the substrate within the active site is restricted; thus, the orientation of the *pro-R* hydrogen of the CoA substrate is different from that found in MCAD. Therefore, the optimum position of the catalytic carboxylate base will, by necessity, be different in IVD than in MCAD. By positioning the catalytic base on helix G of IVD (E254), nature has met this requirement. In this position, the *pro-R* protons at C_α and C_β of the branched chain substrate can correctly align with the carboxylate of the catalytic base and N_5 of the isoalloxazine ring, thus allowing the dehydrogenation reaction to occur efficiently. It should be noted that a double mutant of IVD in which the catalytic base is located on loop JK (E54G/A375E; homologous to the position of the catalytic base in MCAD) retains the same percentage of activity as the wild-type enzyme toward hexanoyl-CoA, a straight-chain substrate. In contrast, the activity of the mutant enzyme toward isovaleryl-CoA is reduced to just 4% of that observed for the wild-type enzyme. Although wild-type human IVD is most active toward shorter chain substrates, the position of the catalytic glutamate on helix G is homologous to that postulated for LCAD. The exact structural basis for the location of the catalytic base in LCAD (E261 on Helix G) is not clear and must await the full structural analysis of this enzyme.

Structural Implications of IVA Point Mutations. Isovaleric acidemia (IVA) is an inborn error of leucine metabolism resulting from a deficiency of IVD. Biochemical and molecular studies on fibroblasts from patients with IVA have shown that heterogeneous mutations in the IVD gene are responsible for this defect. In all cases, IVD protein is either inactive or absent in fibroblasts. Two point mutations have been identified in IVA patients leading to single amino acid substitutions in IVD. In one cell line, a mutation leading to an L13P substitution was found on one IVD allele, while no mRNA from the other IVD allele could be detected (Vockley *et al.*, 1991). These fibroblasts show normal synthesis and mitochondrial targeting and import of the mutant precursor IVD subunit but lack detectable IVD activity as measured by a tritium release or ETF fluorescence reduction assay (Ikeda *et al.*, 1985; Vockley, unpublished data). Expression of this mutant cDNA in an *E. coli* system leads to production of a relatively unstable protein which tends to aggregate following induction of the insert. The small amount of stable protein produced is completely devoid of enzymatic activity. Mutant subunits imported into mitochondria *in vitro* are rapidly degraded. These observations suggest that the primary effect of the L13P mutation is to disrupt folding of imported subunits. An examination of the structure of wild-type IVD offers some insight into the behavior of this mutant enzyme. L13 is located near the point where the N-terminus of IVD and MCAD diverge structurally. Mutation of this residue to a proline will likely disrupt the monomer folding in this region, which appears to be unique to IVD. Thus, the newly imported monomers would be expected to produce subunits which can fold less efficiently than wild-type IVD. Alternatively, when tetramers are formed, one might expect that the abnormal folding in the N-terminus of the monomers would have relatively less effect on tetramer stability in IVD than in MCAD, where intermonomer interactions of the N-termini are extremely important. A second IVD point mutation leading to a G170V substitution has been identified in a fibroblast cell line from another patient with IVA. Once again, these cells are devoid of IVD activity as measured by a tritium release or ETF fluorescence reduction assay (Ikeda *et al.*, 1985; Vockley, unpublished results). An IVD cDNA containing this mutation also leads predominantly to the production of aggregated protein. In contrast to the L13P mutation, the G170V mutant

monomers are extremely labile when produced in a reticulocyte lysate system and do not survive long enough to be imported into mitochondria *in vitro* (Vockley *et al.*, 1995; Vockley, unpublished results). G170 lies in the loop between β-strands 3 and 4 and is responsible for the loop formation. This motif appears to be important in folding one of the two β-sheets of the middle domain, which, in turn, maintains the overall tertiary structure of the monomer. Mutation of this residue to a valine would be predicted to lead to detrimental steric interactions with neighboring residues, and the subsequent alteration of the orientation of the two β-sheets with respect to one another would likely interfere with the overall folding of the IVD monomer. This is in agreement with the *in vitro* observations with this mutant.

REFERENCES

Aoyama, T., Ueno, I., Kamijo, T., & Hashimoto, T. (1994) *J. Biol. Chem. 269*, 19088−19094.

Battaile, K., Mohsen, A. A., & Vockley, J. (1996) *Biochemistry 35*, 15356−15363.

Beinert, H. (1963) in *The Enzymes* (Boyer, P., Lardy, H., & Myrback, K., Eds.) Vol. 7, pp 447−473, Academic Press, New York.

Bross, P., Engst, S., Strauss, A. W., Kelly, D., Rashed, I., & Ghisla, S. (1990) *J. Biol. Chem. 265*, 7116−7119.

Brünger, A. (1992) *X-PLOR, Version 3.1*, Howard Hughes Medical Institue and Department of Biophysics and Biochemistry, Yale University, New Haven, CT.

Carson, M. (1996) *RIBBONS Version 2.5*, University of Alabama, Birmingham, AL.

Carter, C. W., Jr., & Carter, C. W. (1979) *J. Biol. Chem. 254*, 12219−12223.

Crane, F. L., & Beinert, H. (1956) *J. Biol. Chem. 218*, 717−731.

Djordjevic, S., Dong, Y., Paschke, R., Frerman, F., Strauss, A., & Kim, J.-J. P. (1994) *Biochemistry 33*, 4258−4264.

Djordjevic, S., Pace, C., Stankovich, M., & Kim, J.-J. (1995) *Biochemistry 34*, 2163−2171.

Gandour, R. D. (1981) *Bioorg. Chem. 10*, 169−176.

Ghisla, S., Thorpe, C., & Massey, V. (1984) *Biochemistry 23*, 3154−3161.

Gregersen, N., Winter, V., Curtis, D., Deufel, T., Mack, M., Hendricks, J., Willems, P. J., Ponzone, A., Parrella, T., Ponzone, R., Ding, J. H., Zhang, W., Chen, Y. T., Kahler, S., Roe, C. R., Kølvraa, S., Schneiderman, K., Andresen, B. S., Bross, P., & Bolund, L. (1993) *Hum. Hered. 43*, 342−350.

Hoskins, D. D. (1966) *J. Biol. Chem. 241*, 4472−4479.

Ikeda, Y., & Tanaka, K. (1983a) *J. Biol. Chem. 258*, 1077−1085.

Ikeda, Y., & Tanaka, K. (1983b) *J. Biol. Chem. 258*, 9477−9487.

Ikeda, Y., Keese, S., & Tanaka, K. (1985) *Proc. Natl. Acad. Sci. U.S.A. 82*, 7081−7085.

Kim, J.-J. P., & Wu, J. (1988) *Proc. Natl. Acad. Sci. U.S.A. 85*, 6677−6681.

Kim, J.-J. P., Wang, M., & Paschke, R. (1993) *Proc. Natl. Acad. Sci. U.S.A. 90*, 7523−7527.

Lee, H. J. K., Wang, M., Paschke, R., Nancy, A., Ghisla, S., & Kim, J.-J. P. (1996) *Biochemistry 35*, 12412−12420.

Lenich, S. C., & Goodman, S. I. (1986) *J. Biol. Chem. 291*, 4090−4096.

Mahler, H. R. (1954) *J. Biol. Chem. 206*, 13−26.

Matsubara, Y., Indo, Y., Naito, E., Ozasa, H., Glassberg, R., Bockley, J., Ikeda, Y., Kraus, J., & Tanaka, K. (1989) *J. Biol. Chem. 264*, 16321−16331.

Matthews, B. (1968) *J. Mol. Biol. 33*, 491−497.

McPherson, A. (1990) *Eur. J. Biochem. 189*, 1−23.

Mohsen, A.-W. A., & Vockley, J. (1995a) *Biochemistry 34*, 10146−10152.

Mohsen, A.-W. A., & Vockley, J. (1995b) *Gene 160*, 263−267.

Nandy, A., Kieweg, V., Kräutle, F.-G., Vock, P., Küchler, B., Bross, P., Kim, J.-J. P., Rashed, I., & Ghisla, S. (1996) *Biochemistry 35*, 12402−12411.

Nishina, Y., Sato, K., Hazekawa, I., & Shiga, K. (1995) *J. Biochem. 117*, 800−808.

Otwinowski, Z., & Minor, W. (1996) in *Methods of Enzymology* (Carter, C. W., Jr., & Sweet, R. M., Eds.) Vol. 276, Academic Press, New York.

Powell, P., & Thorpe, C. (1988) *Biochemistry 27*, 8022−8028.

Rossman, M. G., & Blow, D. M. (1962) *Acta Crystallogr. 15*, 24−31.

Roussel, A., & Cambillau, C. (1993) *TURBO-FRODO Manual (Version 4.2*), Bio-Graphics, Mountain View, CA.

Ruzicka, F. J., & Beinert, H. (1977) *J. Biol. Chem. 252*, 8440−8445.

Steyn-Parve, E. P., & Beinert, H. (1958) *J. Biol. Chem. 233*, 853−861.

Tanaka, K., Budd, M. A., Efron, M. L., & Isselbacher, K. J. (1966) *Proc. Natl. Acad. Sci. U.S.A. 56*, 236−242.

Tanaka, K., Ikeda, Y., Matsubara, Y., & Hyman, D. (1987) *Enzyme 38*, 91−107.

Vockley, J., Parimoo, B., & Tanaka, K. (1991) *Am. J. Hum. Genet. 49*, 147−157.

Vockley, J., Anderson, B. D., Volchemboum, S. L., Battaile, K. P., & Mohsen, A. A. (1995) *Am. J. Hum. Genet. 57*, A184.

Williamson, G., & Engel, P. (1984) *Biochem. J. 218*, 521−529.

Williamson, G., Engel, P., Mizzer, J., Thorpe, C., & Massey, V. (1982) *J. Biol. Chem. 257*, 4314−4320.

Ziegler, D. M. (1985) *Annu. Rev. Biochem. 54*, 305−329.

BI970422U